Article

A Multiwell Discs Appliance Used to Deliver Quantifiable Accelerations and Shear Stresses at Sonic Frequencies

Sarah A. Klemuk [1,*], **Sarah Vigmostad** [2,†], **Kalyan Endapally** [2,†], **Andrew P. Wagner** [2,†] and **Ingo R. Titze** [1,3,†]

[1] Communication Sciences and Disorders, the University of Iowa, Iowa City, IA 52242, USA;
E-Mail: ingo.titze@utah.edu

[2] Department of Biomedical Engineering, the University of Iowa, Iowa City, IA 52242, USA;
E-Mails: sarah-vigmostad@uiowa.edu (S.V.); bme@engineering.uiowa.edu (K.E.);
andrew-wagner@uiowa.edu (A.P.W.)

[3] National Center for Voice and Speech, University of Utah, Salt Lake City, UT 84112, USA

[†] These authors contributed equally to this work.

[*] Author to whom correspondence should be addressed; E-Mail: sarah-klemuk@uiowa.edu;
Tel.: +1-319-335-8718.

Abstract: To mimic *in vivo* vibration of vocal fold cells, we studied the controllability and range of frequency, acceleration, duration, and shear stress in a new bioreactor attachment. The custom multiwell disc appliance fits into a commercially built rheometer, together termed a torsional rheometer bioreactor (TRB). Previous attachments to the TRB were capable of 50–100 Hz vibrations at relatively high strains but were limited to single-sample experiments. The TRB-multiwell disc system accommodates 20 samples in partially fluid-filled wells in an aseptic environment delivering three different acceleration conditions to different samples simultaneously. Frequency and amplitude used to calculate acceleration along with duration and shear stress were controllable and quantifiable using a combination of built-in rheometer sensors, manufacturer software, and smooth particle hydrodynamics (SPH) simulations. Computed shear stresses at the well bottom using SPH in two and three dimensions were verified with analytical approximations. Results demonstrate capabilities of the TRB-multiwell disc system that, when combined with computational modeling, provide quantifiable vibration parameters covering frequencies 0.01–250 Hz, accelerations of 0.02–300 m/s^2, and shear stresses of 0.01–1.4 Pa. It is

well-suited for studying cell function underlying vocal fold lamina propria homeostasis, inflammation, and wound healing under differential vibration conditions.

Keywords: bioreactor; vocal fold; vibration; smooth particle hydrodynamics; rheometer

1. Introduction

When speaking or singing, the extracellular matrix (ECM) and cells of the vocal fold lamina propria experience forces from oscillation and collision [1,2]. The effect of these forces is described by three parameters: frequency, acceleration, and duration. Inertial forces result from repeated acceleration and deceleration, while shear forces result from fixed and free boundary conditions that prevent tissues from deforming uniformly. Under these forces, cells and extracellular matrix (ECM) modify, maintain, and repair the vocal fold lamina propria as part of normal laryngeal function. To excess, however, these force parameters are implicated in the etiology of vocal fatigue, nodules, polyps, or cysts [3,4]. Among school teachers, who are vocally very active, there is an increased propensity of females toward these disorders that is likely related to a higher fundamental frequency in their speech [5,6]. To better understand the underlying mechanisms in this benefit-cost dichotomy in vocal fold vibration, limited vibration regimens to *ex vivo* cell models have been used to study vibration-dependent cellular mechanisms [7–10]. While significant gene and protein changes have been identified, the roles of frequency, acceleration, duration, shear stress (FADS), and their interactions are largely unknown. The most likely reason is the challenges associated with delivering 10- to 100-fold biomimetic ranges for frequency and stress. Moreover, exploration of this FADS parameter space requires many experimental trials. A device with the potential to satisfy these requirements is a custom-modified torsional rheometer-bioreactor (TRB). The TRB is a commercial rheometer (Gemini model, Malvern Instruments, LTD) with appliances to support tissue and cell viability [11–13]. Initial feasibility of the rheometer to deliver shear stresses at low audio frequencies with parallel plate appliances was shown by adjusting sample thickness, plate radius, material viscoelasticity, and motor inertia [11]. Subsequently, a cup and plate system was designed for the TRB, whereby strains were delivered to three-dimensional cell-seeded scaffolds. Strains were 40% at 70 Hz, and non-destructive rheologic testing on the same engineered tissue was carried out [12]. A third configuration, a glass coverslip mounted to the cup or the moving parallel plate of the TRB, delivered shear stresses up to 2200 Pa at 100 Hz to a monolayer of cells. This delivery was under controlled temperature, humidity, and CO_2 conditions using a custom incubator fitted to the commercial rheometer [13].
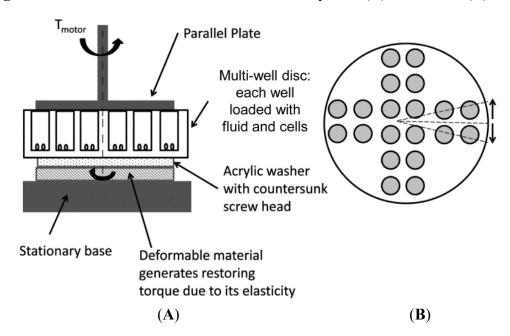
The above investigations demonstrate a high degree of versatility to configure the TRB for single sample experimentation but leave unanswered the challenge to process multiple samples simultaneously. A multiwell disc is evaluated in the current study. It accommodates up to 20 samples in a single experiment. The purposes of this study were to test the TRB's ability to vibrate this multiwell disc at phonation frequencies with accelerations covering a 100-fold range and to computationally determine the range of shear stresses achievable within the partially fluid-filled wells.

2. Experimental Section

2.1. Maximizing Vibration Regimens

The multiwell disc is a commercially manufactured and sterilized 96-well cell-culture plate (BD Biosciences, San Jose, CA, USA) cut into a disc (Medical Instruments, The University of Iowa). The disc diameter is 57 mm, retaining eight usable wells at each of two outer radial positions and four wells at the innermost radial position (Figure 1). It is secured to a standard 45 mm diameter parallel plate (Malvern Instruments, Worcestershire, UK) using the following materials and assembly methods. A center hole in the multiwell disc is drilled that accepts a long center screw (20 mm length and 1.5 mm diameter). Two rubber liners 0.5 mm thick and 45 mm in diameter, with a hole in the middle for the screw to pass through, are used to prevent unwanted slippage and are placed on the bottom and top of the multiwell disc. An acrylic washer measuring 3 mm thick and 45 mm in diameter has a hole drilled through its center with a countersink so the screw head is embedded in the washer and will not make contact with the rheometer base. The acrylic washer and the rubber liners sandwiching the multiwell disc are then fastened to the parallel plate with the long screw threaded into predrilled screw threads at the center of the parallel plate.

Figure 1. Schematics of the multiwell disc assembly, side (**A**) and bottom (**B**) view.

(**A**)   (**B**)

Three acceleration conditions occur for a given experiments. All are at the same frequency and occur simultaneously because of the radial well locations relative to the rotation axis.

Moment of inertia of the multiwell disc assembly is calculated using the equation for a cylinder rotating about a central axis (Equation (1))

$$I = \sum_{1}^{n} \rho_i \pi \ell_i R_i^4 \tag{1}$$

Material density ρ (stainless steel, polycarbonate, acrylic, and rubber), radius R, and length ℓ of each concentric cylinder are included. The inertia for the complete assembly is 1.6×10^{-5} kg m^2.

TRB-multiwell system vibration is achieved by securing the multiwell assembly to a torsional rheometer (Malvern Instruments), then lowering it onto a three-dimensional recoil material (Figure 1). The recoil material supplies a necessary restoring force to the torque motor when operating in oscillation mode. Deformation of the vibrating recoil material transfers to the multiwell disc, resulting in linear displacement within the *x–z* plane if adhesion to the solid surfaces is secure.

The magnitude of displacement is limited by the effective resonance peak of the system as determined by the recoil material's viscoelasticity [11]. Maximal complex strain per unit torque $\gamma*/T*$ of the TRB-multiwell system is written in terms of the angular frequency ω, $G'(\omega)$ and $G''(\omega)$, the elastic and viscous moduli of the recoil material, respectively, and the common radius of the parallel plate and recoil material R

$$\frac{\gamma^*}{T^*} = \frac{1.5}{G'\pi R^3} \frac{1}{1-\left(\dfrac{\omega}{\omega_0}\right)^2 + i\dfrac{G''}{G'}}$$ (2)

where the undamped resonant frequency of the system ω_0 is defined in terms of the elastic modulus, radius, thickness of the recoil material h, and moment of inertia of the entire assembly I:

$$\omega_0^2 = \frac{\pi G' R^4}{2hI}$$ (3)

With the torque (maximum = 0.15 N m), inertia, and radius as fixed parameters, we manipulated the recoil material. Different viscoelastic properties allowed exploitation of the effective resonance of the TRB-multiwell system. Four recoil materials were tested in the present study.

2.2. Using SPH to Model Shear Stresses

Fluid shear stresses within the partially fluid-filled wells of the multiwell disc are not directly measurable. Rather, computational methods were used to quantify this vibration parameter. Smoothed Particle Hydrodynamics (SPH) is a computational technique for calculating the fluid dynamics using a Lagrangian framework. This approach has been validated against many benchmark cases, and is particularly well suited for free-surface flows, such as the TRB-multiwell system. SPH was initially proposed by Lucy [14] and separately by Gingold and Monaghan [15]. Although its first application was in astrophysics, SPH is currently used in the analysis of incompressible and multiphase flow, heat and mass transfer, elasticity, and fracture [16,17].

As opposed to mesh-based computational fluid dynamics (CFD) approaches, SPH is a mesh-free method based on interpolation theory. In this method, matter is divided into a set of interpolation points or particles. Material properties such as density and viscosity, as well as the field variables velocity, pressure, and stress, are assigned to the particles. Integral interpolation among these particles approximates the field variables,

$$f(\mathrm{x}) = \int_\Omega f(\mathrm{x}')\delta(\mathrm{x}-\mathrm{x}')dx'$$ (4)

where $\delta(\mathrm{r}-\mathrm{r}')$ is the Dirac delta function and Ω is the computational domain. The Dirac delta function can be approximated by a weight or kernel function $\mathrm{W}(\mathrm{r}-\mathrm{r}', \mathrm{h})$, where h is the smoothing length. Assigning A(r) as a field variable of the spatial coordinates, the integral representation of A(r) becomes

$$\langle A(\mathbf{r}) \rangle = \int_{\Omega} A(\mathbf{r}') \; W(\mathbf{r} - \mathbf{r}', h) \; d\mathbf{r}' \tag{5}$$

If A(r′) is known only at a discrete set of N points r_1, r_2,..., r_N, the interpolation of quantity A(r) can be approximated by a summation interpolant,

$$\langle A_h(\mathbf{r}) \rangle = \sum_{b=1}^{N} \frac{m_b}{\rho_b} A_b \, W(\mathbf{r} - \mathbf{r}', h) \tag{6}$$

where the basic properties of the kernel function are defined as

$$\int W(x - x', h) dx' = 1,$$
$$\lim_{h \to 0} W(x - x', h) = \delta(x - x') \tag{7}$$

The final equation used in the present investigation is a cubic spline kernel that is frequently used in SPH simulations. The compact support of this kernel function is equal to *2h*, meaning that the interactions vanish for *r > 2h*

$$M_4(x) = \frac{1}{6} \begin{cases} (2-s)^3 - 4(1-s)^3 & , \quad 0 \le s \le 1 \\ (2-s)^3 & , \quad 1 \le s \le 2 \\ 0 & , \quad s > 2 \end{cases} \tag{8}$$

2.3. Recoil Material Evaluation

Selection of recoil materials for empirical studies was based on predicted viscoelastic properties that could generate TRB-multiwell system accelerations of 10–1000 m/s². To predict properties at these accelerations, we calculated G' and G″ with analytic expressions [11]. Rewriting complex strain γ^* as acceleration, we assume the small angle approximation $r\theta = \gamma d$ where *r* is radial distance from the center of rotation, θ is angular displacement, and *d* is sample thickness. Using the second derivative of sinusoidal motion $e^{i\omega t}$ at angular frequency ω,

$$|\ddot{A}| = d\gamma\omega^2 \tag{9}$$

we get

$$G' = \frac{1.5}{\pi R^3} d\omega^2 \left(\frac{T}{\ddot{A}} \cos\phi + \frac{I}{0.75R} \right) \tag{10}$$

$$G'' = \frac{1.5}{\pi R^3} d\omega^2 \frac{T}{\ddot{A}} \sin\phi \tag{11}$$

where R is the sample radius and ϕ is the phase shift due to viscous drag of the sample. Four recoil materials were tested: a dimethyl silicon polymer, hot melt pressure sensitive adhesive (arranged in a ring), double-sided white foam tape, and removable foam mounting squares. Each sufficiently adhered to solid fixtures, with no signs of slippage. Linear viscoelasticity (LVE) of each material across frequency using a 45 mm diameter parallel plate and stationary base, and accelerations at maximum torque across frequency using the TRB-multiwell system were measured. As per standard LVE protocol, each recoil material was trimmed to the size of the parallel plate. An amplitude sweep was

performed at 1 Hz; a strain, resulting in constant elastic and viscous moduli, was then chosen for small amplitude deformation and subsequent collection of *G'* and *G''* values at frequencies 0.1–100 Hz [18]. For acceleration measures, strain data (1–250 Hz) at the ¾ radius position and maximum torque were recorded, then converted to accelerations, using Equation (9) and the respective sample thickness and angular frequency.

2.4. Shear Stress Modeling

Shear stresses within each well of the multiwell disc were computed during vibration conditions using the SPH model described above. The fluid within a well (radius = 3.25 mm, height = 12.1 mm), was modeled as a 2D particle array—60 × 129 for 100 μL or 30 × 129 for 50 μL of fluid—to oscillate with a given frequency and amplitude. Fluid density (1 g/cm^3) was fixed. Fluid viscosity of cell culture medium, measured in triplicate with the rheometer, was 2.26 ± 0.13 mPa s. We also tested the model using a viscosity three times that of cell culture medium. Computations were repeated for several simulation cycles of vibration to ensure a time-independent solution. Shear stresses were then calculated for particle arrays.

To validate simulation results, we analytically determined a classical fluid-mechanics benchmark, the Stokes Second Problem. Stokes Second Problem describes oscillatory movement of a fluid that is bounded on the bottom by an infinitely long plane, freely bound on the top, and has no side walls. Oscillatory flow begins at time *t* at a particular frequency *n* (Figure 2). The velocity field *u* is governed by the equation

$$\frac{du}{dt} = v\frac{d^2u}{dy^2} \tag{12}$$

where v is the kinematic viscosity. Initial boundary conditions are

$$u(0,t) = \begin{cases} 0 & \text{for } t \le 0 \\ U\cos(nt) & \text{for } t > 0 \end{cases} \tag{13}$$

$$u(y,t) = \text{ finite}$$

The analytical solution of the Stokes Second Problem is

$$\frac{u(y,t)}{U} = \exp\left(-\sqrt{\frac{n}{2v}}y\right)\cos\left(nt - \sqrt{\frac{n}{2v}}y\right) \tag{14}$$

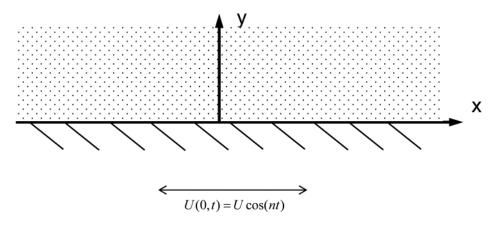For a Newtonian fluid, the shear stress is directly proportional to the strain rate

$$\tau = \mu\frac{du}{dy} \tag{15}$$

so by finding the derivative of Equation (14) we can approximate the shear stress,

$$\tau_{xy} = \frac{du(y,t)}{dy} = kU\exp(ky)[\cos(nt + ky) - \sin(nt + ky)] \tag{16}$$

where $k = -\sqrt{n/2v}$.

Figure 2. Schematic of Stokes Second Problem; a semi-infinite surface begins oscillation at time *t* with a frequency *n*.

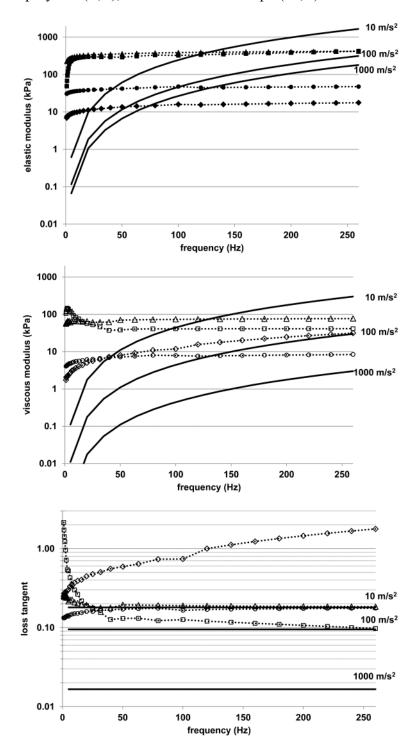$$U(0,t) = U\cos(nt)$$

3. Results and Discussion

3.1. Viscoelastic Properties of Recoil Materials

To predict optimal properties of potential recoil materials, we calculated viscoelastic moduli for specific accelerations using Equations (10) and (11) with a nominal phase shift ϕ of 0.2. Elastic and viscous moduli should range from 30 to 2000 kPa and 0.5 to 300 kPa, respectively, and loss tangents (ratio of viscous to elastic moduli) should range from 0.02 to 0.2 to achieve 10–1000 m/s^2 acceleration at 100–250 Hz (solid lines in Figure 3). Properties of the four tested recoil materials fell within these ranges. Their elastic and viscous moduli were 1.3–350 kPa and 1.1–140 kPa, respectively (symbols with dotted lines in Figure 3 top and middle). Direct measures were accurate up to 100 Hz and then extrapolated to 250 Hz using line fits (Table 1).

Table 1. Linear fit equations with highest R^2 and corresponding coefficients used to extrapolate viscoelastic values of recoil materials to 250 Hz.

	Double-sided foam tape	Dimethyl silicon	Removable mounting squares	Hot melt pressure sensitive adhesive
Elastic modulus				
Freq range of data used in extrapolation (Hz)	0.1–100	10–100	0.1–100	0.1–100
Line fit function	$y = a\ln(x) + b$	$y = ae^{bx}$	$y = ax^b$	$y = ax^b$
a (Pa)	34,669	279,045	30,709	6877
b (Pa)	225,278	0.0016	0.078	0.1689
R^2	0.9961	0.7644	0.9818	0.9952
Viscous modulus				
Freq range of data used in extrapolation (Hz)	0.1–100	32–100	0.1–100	0.1–100
Line fit function	$y = a\ln(x) + b$	$y = ax + b$	$y = ax^b$	$y = ax + b$
a (Pa)	4079.9	−11.813	4187.9	112.83
b (Pa)	54098	41086	0.1237	1899.6
R^2	0.7611	0.0105	0.9607	0.9631

Figure 3. Predicted shear elastic moduli (**top**) and viscous modulus (**middle**) and loss tangent (viscous modulus/elastic modulus) (**bottom**) achieve multiwell disc accelerations of 10–1000 m/s^2 (solid lines). Measured shear elastic modulus (**top**) and viscous modulus (**middle**), and loss tangent (**bottom**) of four different recoil materials: hot melt pressure sensitive adhesive (arranged in a ring) (♦,◊), removable foam mounting squares (●,○), dimethyl silicon polymer (■,□), double-sided foam tape (▲,Δ).
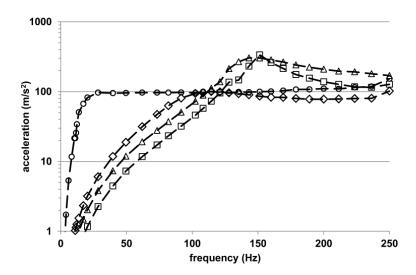

Loss tangent values were usually less than 0.2 across frequency. Exceptions to this dominance of elasticity over viscosity were for the dimethyl silicon polymer at frequencies less than 2.5 Hz and the hot melt pressure sensitive adhesive at frequencies greater than 100 Hz.

3.2. TRB-Multiwell Disc Accelerations

Accelerations of the TRB-multiwell disc system are shown in Figure 4. All four materials generated accelerations of 50 m/s^2 or more at frequencies over 100 Hz. The greatest accelerations were obtained using the two stiffest recoil materials. Peak accelerations were 336 and 303 m/s^2 at 151 Hz using the dimethyl silicon polymer (squares) and foam tape (triangles), respectively. Up to 250 Hz, the foam tape maintained slightly higher accelerations (285–170 m/s^2) compared to the dimethyl silicon polymer (285–115 m/s^2). At frequencies below 100 Hz, accelerations of the TRB-multiwell disc system were maximal when using the mounting squares (circles) as the recoil material. Accelerations of 100 m/s^2 were achieved and sustained beginning at 28 Hz through 250 Hz. The hot melt pressure sensitive adhesive (diamonds) was the least effective at maximizing accelerations, both below and above 100 Hz, compared to the other three recoil materials. Peak accelerations were 100 m/s^2 at 115 Hz and stayed above 78 m/s^2 through 250 Hz.

Figure 4. Measured accelerations of the torsional rheometer bioreactor (TRB)-multiwell system using maximum torque and specified recoil material: hot melt pressure sensitive adhesive (◊) and removable foam mounting squares (○), dimethyl silicon polymer (□), and double-sided foam tape (Δ) meet and exceed expectations over a broad frequency range.

Tables 2 and 3 summarize approximate viscoelastic properties of recoil materials (to one significant figure) that produced target accelerations at frequencies 2–250 Hz. The values correspond to the four materials tested in the current study. The tables serve as references for future investigators interested in using other recoil materials for the TRB.

3.3. Stokes Second Equation Comparisons

A total of four different combinations of frequency and amplitude were determined analytically from Stokes second equation and compared to two-dimensional and three-dimensional SPH simulations. Shown in Table 4, 2D and 3D SPH stress values were comparable. 2D simulations required considerably less computation time than 3D simulations so they were used for the remainder of the conditions. Results from Stokes Second Problem were higher but within the same order of magnitude as those of the simulations. This result is consistent with a study by Khan and

colleagues [19]. They compared analytic solutions of an oscillating fluid between two sidewalls to that without side walls. The reduced amplitude was attributed to increasing shear forces at the wall boundary, which causes the velocity to die out early as it approaches zero at the wall boundary.

Table 2. Approximate elastic moduli of recoil materials (in kPa) to achieve target accelerations at frequencies 2–250 Hz (e.g., to generate 100 m/s^2 at 200 Hz, the recoil material's elastic modulus is between 50 and 400 kPa).

Acceleration (m/s²)	0.4	1	2	5	10	15	20	40	60	80	100	200	300
Frequency (Hz)	Approximate Elastic Modulus of Recoil Materials (kPa)												
2	30												
4		30											
6		30											
8	10–300	10–35	30										
10	10–300				40								
20	11–300					40							
50		10–400			10–40		40						
80				10–400				10–50		50			
100					20–400					20–50			
130						20–400						400	
150						20–400						400	
180						20–400						400	
200						20–400					50–400	400	
220						20–400					50–400	400	
250						20–400						50–400	

Table 3. Approximate viscous moduli of recoil materials (in kPa) to achieve target accelerations at frequencies 2–250 Hz (e.g., to generate 100 m/s^2 at 200 Hz, the recoil material's viscous modulus is between 8 and 80 kPa).

Acceleration (m/s²)	0.4	1	2	5	10	15	20	40	60	80	100	200	300
Frequency (Hz)	Approximate Viscous Modulus of Recoil Materials (kPa)												
2	4												
4		5											
6		5											
8	3−70	3−5	5										
10	4−60				5								
20	5−60					6							
50		7−70			7−8		7						
80				8−70				8−10		8			
100					8−70					8−10			
130						8−70						70	
150						8−70						40−70	
180						8−70						40−70	
200						8−80						80	
220						8−80						80	
250						8−80						80	

Table 4. Comparison of 2D, 3D and Stokes Second Problem results.

Frequency and amplitude conditions	2D SPH	3D SPH	Stokes 2nd problem
	Shear stress (Pa)		
126 Hz; 0.46 mm	0.3	0.5	1.6
126 Hz; 0.069 mm	0.05	0.06	0.5
220 Hz; 0.063 mm	0.07	0.1	0.2
220 Hz; 0.0094 mm	0.01	0.03	0.08

3.4. Simulation of Shear Stress

Smooth particle hydrodynamics (SPH) results showed that shear stresses reached steady state after a single vibration cycle (Figure 5). Largest stresses were computed at the well bottom and stress magnitude diminished with vertical distance. In all, 17 different cases were simulated, varying frequency, amplitude of vibration, fluid viscosity, and fluid volume. As shown in Figure 6, an increase in acceleration (by increasing frequency or amplitude) increased shear stress proportionally. Alternatively, a three-fold viscosity increase quadrupled shear stress. Halving the fluid volume increased shear stress by 1.5–4.5 times, depending on the acceleration. In summary, resulting fluid shear stresses, shown in Figure 6, span a 100-fold range, from 0.01 to 1.35 Pa.

Figure 5. Smooth particle hydrodynamics (SPH) computational shear stress solutions in two dimensions reach a steady state after one cycle. Largest stress occurs at the well bottom and diminishes with vertical distance from the moving surface.
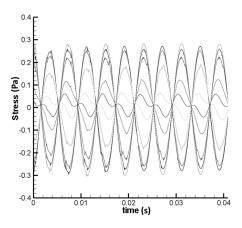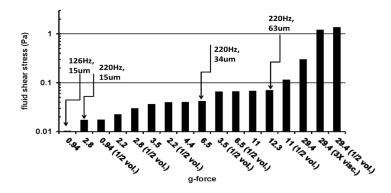

Figure 6. Tunable shear stresses inside the partially filled wells of the multiwell disc span a 100-fold range, as determined by SPH simulations. Tunable features include frequency, amplitude, fluid volume, and fluid viscosity.

4. Conclusions

The multiwell disc appliance facilitates exploration of a frequency, acceleration, duration, shear (FADS) parameter space that has been rendered too time consuming and expensive with previously designed vibrating bioreactors. Our data demonstrate maximum accelerations of 9.2–334 m/s^2 at 100–250 Hz by using different recoil materials with the TRB-multiwell system. These accelerations are much lower than predicted vocal fold accelerations using three-mass computer simulation or stroboscopy data (1000–4000 m/s^2 at 100–400 Hz) [20,21] but they are the highest values generated by any bioreactor to date [7,8,10,22–26]. Stiff recoil materials provide accelerations in the order of 300 m/s^2 above 100 Hz and more compliant materials provide 100 m/s^2 at 28–100 Hz vibrations.

The large range of accelerations of the multiwell disc is made possible due to one main factor. The viscoelastic properties of the added recoil materials allow a mechanical resonance of the oscillating motor over a broad frequency range. The factory-designed torsional rheometers require the test sample stiffness to generate a recoil force for oscillatory motion. For low stiffness test materials, particularly when operating at higher frequencies, the motor shaft and plate spin instead of oscillate. Previously, we showed that the effective resonance of a rheometer-sample system shifts along the frequency axis depending on the sample radius, thickness, and the unknown elastic modulus [11]. Accurate viscoelastic measurements were achieved over a greater frequency range (up to and below the resonant peak produced by test sample stiffness) by increasing the sample radius or decreasing the sample thickness, or some combination of these variables. An increase in the sample radius or loss tangent reduces the resonant peak height and increases its width.

By adding a recoil material with known stiffness, we showed here that a system resonance could be exploited to provide a greater frequency range over which desired accelerations could be achieved. The viscoelastic properties of four recoil materials were tested to provide a two order of magnitude range of accelerations.

Shear stress is the last component in FADS parameter space we took into account when simulating vocal fold vibration conditions in the TRB. The partially filled wells of the multiwell disc exposed cells to shear stress, but measuring the stresses directly was not possible. Rather, using smooth particle hydrodynamics (SPH), we computed shear stresses in two dimensions—values comparable to those in three-dimensional simulations but with less computational expense. The resulting shear stresses of 0.01–1 Pa were tunable by altering frequency, amplitude, viscosity, or fluid volume in the TRB-multiwell disc system.

Direct measures of shear stress within vibrating vocal fold tissue are not currently possible. Furthermore, until now, shear stresses within a bioreactor have not been a controllable parameter from which to systematically investigate vocal fold cell function or tissue remodeling. Target shear stresses of 100–1000 Pa in previous appliance designs were consistent with stresses reported in physical and computational models and with constitutive relationships of bulk vocal fold deformation [2,27–29]. Multiwell disc stresses, however, were 100-fold lower than this target, just as achievable accelerations were much less than what is estimated during vocal fold oscillation.

While this outcome might appear to be a significant limitation to the TRB-multiwell disc system, preliminary results from our lab show vocal fold fibroblast sensitivities to these ranges (see Appendix Materials). We tested effects of FADS when vocal fold fibroblast cells first established ECM

connectivity, a time scale that corresponds to events in early wound healing and in cell migration [30–34]. In particular, cellular focal adhesions to ECM transduce kinetic to biochemical signaling and regulate cell motility, genetic messaging, and matrix remodeling [35–38], making cell adhesion a strong candidate for initial investigations into FADS-sensitive mechanobiology.

Future knowledge from studies using the TRB-multiwell disc system could extend beyond that of vocal fold cellular and tissue function. Skin and brain are two organ systems with known exposures to forces comparable to that of vocal fold tissue—forces transferred to embedded cells with comparable magnitudes due to similar viscoelastic properties of the tissues [39–41]. Persons operating heavy hand-held equipment can experience adverse effects such as Hand-Arm Vibration Syndrome if frequency, acceleration, and duration safety limits are exceeded [21,42,43]. Greater understanding of neuronal mechanobiology in the presence of tool-transmitted vibrations, at 28–100 Hz vibrations and 100 m/s^2 accelerations, could be realized using the more compliant drivers with the TRB-multiwell disc system, as exemplified in Figure 4. In the brain, endogenous neural mechanobiology is not well understood, nor is there good understanding of the cellular-molecular responses to traumatic brain injury [44,45]. A finding that the neuropeptide galanin has protective functions against shear stress of cortical neurons was determined using a microfluidics device [46]. The stresses with that device are a subset of the quantitative FADS parameters possible with the TRB-multiwell disc system. Controls on the rheometer permit single or short duration pulsing to simulate blunt trauma forces, or duty ratio-to-continuous low frequency motion to simulate endogenous conditions on multiple samples simultaneously. Particularly for systems such as the brain and vocal fold, forces are complex and knowledge of their mechanobiology is limited. A device such as the TRB-multiwell disc system can provide an invaluable tool, quantifying forces to gain understanding of cell behavior directly related to FADS parameters.

Acknowledgments

Conflicts of Interest

The authors declare no conflict of interest.

Appendix

1. Supplemental Experimental Section: Fibroblast Adhesion

1.1. Cell Culture and Adhesion Assay

An immortalized vocal fold fibroblast cell line was used for adhesion studies, originating from a 21 y.o. male (young adult cell line, hVFFCs) [47,48]. Cells were cultured in a 37 °C, 5% CO_2 atmosphere in Dulbecco's modified Eagle medium (DMEM), high glucose with glutamine, 10%

heat-inactivated fetal bovine serum (FBS). The day prior to experimentation, cells were lifted using trypsin and replated into flasks, then removed the following day using an enzyme-free dissociation solution known to minimize the disturbance of cell surface proteins (Gibco, Carlsbad, CA, USA). Cells were then treated with Calcein AM (calcein acetoxymethyl ester) (Invitrogen Corporation, Carlsbad, CA, USA) to fluorescently tag adherent cells. Twenty wells in two the multiwell discs (one experimental and one control) were coated with 0.5 µg/mL fibronectin with 100 µL per well and stored overnight.

The day of the experiment, the fibronectin-coated wells were washed with PBS. 100 µL of Calcein AM-treated cells (10^6 cells/mL) were placed in each coated well using complete cell culture medium. Experimental conditions commenced 30 min later. Upon completion of a prescribed vibration regimen, the experimental and control multiwell discs were removed from their TRB. Each well was washed 3 times with PBS so only adhered cells remained, inverted for 5 min to dry, and replenished with 200 µL of PBS. Optical density (*i.e.*, fluorescent intensity) was measured for each disc (absorption wave length = 490 nm; emission wave length = 525 nm) along with serial dilution wells (prepared similarly to the discs but maintained in a standard incubator during testing) using a FLUOstar Omega microplate reader (BMG Labtech; Durham, NC, USA).

1.2. Vibration Regimens

Selection of vibration regimens mimicked human voice use. Frequencies were male and female fundamental frequencies (126 and 220 Hz respectively). ON/OFF vibration duty ratios were 0.55 (0.55 s ON and 0.45 s OFF), corresponding to voiced-unvoiced characteristics of spoken American English and recorded during daily voice use of public school teachers [49]. The test duration was also similar to teacher-student contact time (4.4–6.4 h). Accelerations covered a 10-fold range (9.8–111 m/s^2). To reduce the four vibration parameters (frequency, duration, acceleration, stress) down to two, we used a metric proposed by Titze *et al.* for vocal fold vibration: cumulative distance (*i.e.*, vocal dose)

$$\text{distance} = 4 A_{rms} F_0 t \tag{A1}$$

where A_{rms} is the root mean square amplitude of movement (converted from the acceleration), F_0 is the frequency and t is duration of voicing [21]. The three variables are measured by the high precision torque motor and sensing system of the rheometer, quantifying input and output vibrations every second for the duration of each experiment. Shear stress is determined computationally, as explained previously. A total of twelve cumulative distances covering a 10-fold range (47–550 m) were tested.
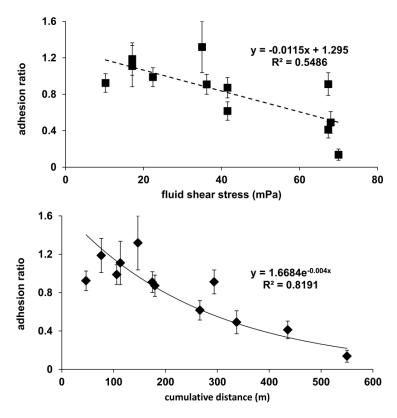
1.3. Adhesion Ratio Calculation

Adherence changes due to vibration regimens were reported as the adhesion ratio. Measured optical density, from each well containing cells, was divided by the mean optical density of the control wells (*N* = 20). All experiments were conducted with multiple samples; at the outermost and middle positions of the experimental multiwell disc *N* = 8, and at the innermost position of the experimental multiwell *N* = 4. Standard deviation for each mean adhesion ratio was calculated using propagation of errors, then dividing by the square root of *N* to obtain the standard error of the mean [50].

2. Supplementary Results

2.1. Adhesion Sensitivity to Vibration

Human vocal fold fibroblast cells were tested for their early adhesion abilities (within 7 h of initially plating cells on fibronectin) in the multiwell disc under a variety of vibration conditions. The adhesion ratio (experimental/control emitted optical density) diminished linearly with calculated shear stress and diminished exponentially as a function of cumulative distance (Figure A1). Adhesion ratios were consistently greater than 0.9 when cumulative distances were less than 160 m and shear stresses were less than 40 mPa.

Figure A1. Mean early adhesion ratio of human vocal fold fibroblast cells (within 7 h of initial plating on fibronectin) as a function of shear stress (**top**) and cumulative distance (**bottom**). Error bars correspond to standard error of the mean. Linear (**top**) and exponential (**bottom**) fits, their coefficients and goodness of fit are listed.

References

1. Titze, I.R. Mechanical stress in phonation. *J. Voice* **1994**, *8*, 99–105.
2. Tao, C.; Jiang, J.J. Mechanical stress during phonation in a self-oscillating finite-element vocal fold model. *J. Biomech.* **2007**, *40*, 2191–2198.
3. Solomon, N.P. Vocal fatigue and its relation to vocal hyperfunction. *Int. J. Speech-Lang. Pathol.* **2008**, *10*, 254–266.
4. Thibeault, S.L. Advances in our understanding of the Reinke space. *Curr. Opin. Otolaryngol. Head Neck Surg.* **2005**, *13*, 148–151.

5. Hunter, E.J.; Tanner, K.; Smith, M.E. Gender differences affecting vocal health of women in vocally demanding careers. *Logop. Phoniatr. Vocol.* **2011**, *36*, 128–136.

6. Roy, N.; Merrill, R.M.; Thibeault, S.; Gray, S.D.; Smith, E.M. Voice disorders in teachers and the general population: effects on work performance, attendance, and future career choices. *J. Speech Lang. Hear. Res.* **2004**, *47*, 542–551.

7. Gaston, J.; Quinchia Rios, B.; Bartlett, R.; Berchtold, C.; Thibeault, S.L. The response of vocal fold fibroblasts and mesenchymal stromal cells to vibration. *PLoS One* **2012**, *7*, e30965.

8. Titze, I.R.; Hitchcock, R.W.; Broadhead, K.; Webb, K.; Li, W.; Gray, S.D.; Tresco, P.A. Design and validation of a bioreactor for engineering vocal fold tissues under combined tensile and vibrational stresses. *J. Biomech.* **2004**, *37*, 1521–1529.

9. Webb, K.; Li, W.; Hitchcock, R.W.; Smeal, R.M.; Gray, S.D.; Tresco, P.A. Comparison of human fibroblast ECM-related gene expression on elastic three-dimensional substrates relative to two-dimensional films of the same material. *Biomaterials* **2003**, *24*, 4681–4690.

10. Wolchok, J.C.; Brokopp, C.; Underwood, C.J.; Tresco, P.A. The effect of bioreactor induced vibrational stimulation on extracellular matrix production from human derived fibroblasts. *Biomaterials* **2009**, *30*, 327–335.

11. Titze, I.R.; Klemuk, S.A.; Gray, S. Methodology for rheological testing of engineered biomaterials at low audio frequencies. *J. Acoust. Soc. Am.* **2004**, *115*, 392–401.

12. Klemuk, S.A.; Jaiswal, S.; Titze, I.R. Cell viability viscoelastic measurement in a rheometer used to stress and engineer tissues at low sonic frequencies. *J. Acoust. Soc. Am.* **2008**, *124*, 2330–2339.

13. Titze, I.R.; Klemuk, S.A.; Lu, X. Adhesion of a monolayer of fibroblast cells to fibronectin under sonic vibrations in a bioreactor. *Ann. Otol. Rhinol. Laryngol.* **2012**, *121*, 364–374.

14. Lucy, L. A numerical approach to the testing of the fission hypothesis. *Astron. J.* **1977**, *82*, 1013–1024.

15. Gingold, R.; Monaghan, J. Smoothed particle hydrodynamics-theory and application to non-spherical stars. *Mon. Notices R. Astron. Soc.* **1977**, *181*, 375–389.

16. Monaghan, J. Smoothed particle hydrodynamics. *Rep. Prog. Phys.* **2005**, *68*, 1703.

17. Liu, M.; Liu, G. Smoothed particle hydrodynamics (SPH): An overview and recent developments. *Arch. Comput. Methods Eng.* **2010**, *17*, 25–76.

18. Ferry, J.D. *Viscoelastic Properties of Polymers*; John Wiley & Sons: New York, NY, USA, 1980.

19. Khan, M.; Iftikhar, F.; Anjum, A. Some unsteady flows of a jeffrey fluid between two side walls over a plane wall. *Z. Fur Naturforschung Sect. A* **2011**, *66*, 745–752.

20. Horacek, J.; Laukkanen, A.M.; Sidlof, P.; Murphy, P.; Svec, J.G. Comparison of acceleration and impact stress as possible loading factors in phonation: A computer modeling study. *Folia Phoniatr. Et Logop.* **2009**, *61*, 137–145.

21. Titze, I.R.; Svec, J.G.; Popolo, P.S. Vocal dose measures: Quantifying accumulated vibration exposure in vocal fold tissues. *J. Speech Lang. Hear. Res.* **2003**, *46*, 919–932.

22. Van Dyke, W.S.; Sun, X.; Richard, A.B.; Nauman, E.A.; Akkus, O. Novel mechanical bioreactor for concomitant fluid shear stress and substrate strain. *J. Biomech.* **2012**, *45*, 1323–1327.

23. Wolchok, J.C.; Tresco, P.A. The isolation of cell derived extracellular matrix constructs using sacrificial open-cell foams. *Biomaterials* **2010**, *31*, 9595–9603.

24. Bacabac, R.G.; Smit, T.H.; van Loon, J.J.W.A.; Boulabi, B.Z.; Helder, M.; Klein-Nulend, J. Bone cell responses to high-frequency vibration stress: Does the nucleus oscillate within the cytoplasm? *FASEB J.* **2006**, *20*, 858–864.

25. Titze, I.R.; Broadhead, K.; Tresco, P.A.; Gray, S. Strain distribution in an elastic substrate vibrated in a bioreactor for vocal fold tissue engineering. *J. Biomech.* **2005**, *38*, 2406–2414.

26. Kutty, J.K.; Webb, K. Vibration stimulates vocal mucosa-like matrix expression by hydrogel-encapsulated fibroblasts. *J. Tissue Eng. Regen. Med.* **2010**, *4*, 62–72.

27. Jiang, J.J.; Titze, I.R. Measurement of vocal fold intraglottal pressure and impact stress. *J. Voice* **1994**, *8*, 132–144.

28. Gunter, H.E. A mechanical model of vocal-fold collision with high spatial and temporal resolution. *J. Acoust. Soc. Am.* **2003**, *113*, 994–1000.

29. Chen, L.-J.; Mongeau, L. Verification of two minimally invasive methods for the estimation of the contact pressure in human vocal folds during phonation. *J. Acoust. Soc. Am.* **2011**, *130*, 1618–1627.

30. Gupton, S.L.; Waterman-Storer, C.M. Spatiotemporal feedback between actomyosin and focal-adhesion systems optimizes rapid cell migration. *Cell* **2006**, *125*, 1361–1374.

31. Lim, X.; Tateya, L.; Tateya, T.; Munoz-Del-Rio, A.; Bless, D.M. Immediate inflammatory response and scar formation in wounded vocal folds. *Ann. Otol. Rhinol. Laryngol.* **2006**, *115*, 921–929.

32. Ling, C.; Raasch, J.L.; Welham, N.V. E-Cadherin and transglutaminase-1 epithelial barrier restoration precedes type IV collagen basement membrane reconstruction following vocal fold mucosal injury. *Cells Tissues Organs* **2011**, *193*, 158–169.

33. Welham, N.V.; Lim, X.; Tateya, I.; Bless, D.M. Inflammatory factor profiles one hour following vocal fold injury. *Ann. Otol. Rhinol. Laryngol.* **2008**, *117*, 145–152.

34. Zaidel-Bar, R.; Cohen, M.; Addadi, L.; Geiger, B. Hierarchical assembly of cell-matrix adhesion complexes. *Biochem. Soc. Trans.* **2004**, *32*, 416–420.

35. Burridge, K.; Chrzanowska-Wodnicka, M. Focal adhesions, contractility, and signaling. *Annu. Rev. Cell Dev. Biol.* **1996**, *12*, 463–519.

36. Matthews, B.D.; Overby, D.R.; Mannix, R.; Ingber, D.E. Cellular adaptation to mechanical stress: Role of integrins, Rho, cytoskeletal tension and mechanosensitive ion channels. *J. Cell Biol.* **2006**, *119*, 508–518.

37. Schwartz, M.A. Integrins and Extracellular Matrix in Mechanotransduction. *Cold Spring Harb. Perspect. Biol.* **2010**, *2*, doi:10.1101/cshperspect.a005066.

38. Jamney, P.A.; McCulloch, C.A. Cell mechanics: Integrating cell responses to mechanical stimuli. *Annu. Rev. Biomed. Eng.* **2007**, *9*, 1–34.

39. Arbogast, K.B.; Margulies, S.S. Material characterization of the brainstem from oscillatory shear tests. *J. Biomech.* **1998**, *31*, 801–807.

40. Holt, B.; Tripathi, A.; Morgan, J. Viscoelastic response of human skin to low magnitude physiologically relevant shear. *J. Biomech.* **2008**, *41*, 2689–2695.

41. Chan, R.W. Measurements of vocal fold tissue viscoelasticity: Approaching the male phonatory frequency range. *J. Acoust. Soc. Am.* **2004**, *115*, 3161–3170.

42. McLeod, R.W.; Griffin, M.J. Effects of whole-body vibration waveform and display collimation on the performance of a complex manual control task. *Aviat. Space Environ. Med.* **1990**, *61*, 211–219.

43. Dahlin, L.B.; Necking, L.E.; Lundstrom, R.; Lundborg, G. Vibration exposure and conditioning lesion effect in nerves: An experimental study in rats. *J. Hand Surg.* **1992**, *17*, 858–861.

44. Tyler, W.J. The mechanobiology of brain function. *Nat. Rev. Neurosci.* **2012**, *13*, 867–878.

45. LaPlaca, M.C.; Prado, G.R. Neural mechanobiology and neuronal vulnerability to traumatic loading. *J. Biomech.* **2010**, *43*, 71–78.

46. Liu, M.; Song, W.; Li, P.; Huang, Y.; Gong, X.; Zhou, G.; Jia, X.; Zheng, L.; Fan, Y. Galanin protects against nerve injury after shear stress in primary cultured rat cortical neurons. *PLoS One* **2013**, *8*, e63473.

47. Chen, X.; Thibeault, S.L. Characteristics of age-related changes in cultured human vocal fold fibroblasts. *Laryngoscope* **2008**, *118*, 1700–1704.

48. Chen, X.; Thibeault, S.L. Novel isolation and biochemical characterization of immortalized fibroblasts for tissue engineering vocal fold lamina propria. *Tissue Eng. C* **2009**, *15*, 201–212.

49. Titze, I.R.; Hunter, E.; Svec, J.G. Voicing and silence periods in daily and weekly vocalizations of teachers. *J. Acoust. Soc. Am.* **2007**, *121*, 469–478.

50. Bevington, P.R.; Robinson, K.D. *Data Reduction and Error Analysis for the Physical Sciences*; Tubb, S.J., Morriss, J.M., Eds.; McGraw-Hill, Inc.: New York, NY, USA, 1992; pp. 1–328.